


ORIGINAL ARTICLE

CD205⁺ polymorphonuclear myeloid-derived suppressor cells suppress antitumor immunity by overexpressing GLUT3

Chenghao Fu¹ | Zhonglin Fu² | Chunying Jiang² | Chao Xia² | Yiwei Zhang² | Xingju Gu² | Kexin Zheng¹ | Dayu Zhou² | Shuang Tang² | Shuxia Lyu^{1,2} | Shiliang Ma² 

¹College of Food Science, Shenyang Agricultural University, Shenyang, China

²College of Bioscience and Biotechnology, Shenyang Agricultural University, Shenyang, China

Correspondence

Shiliang Ma, College of Bioscience and Biotechnology, Shenyang Agricultural University, 110866 Shenyang, China.
Email: msl@syau.edu.cn

Shuxia Lyu, College of Food Science, Shenyang Agricultural University, 110866 Shenyang, China.
Email: lushuxia@syau.edu.cn

Present address

Zhonglin Fu, Institutes for Translational Medicine, Soochow University, Suzhou, China

Funding information

"Financial Support for Selected Researchers Back from Abroad (2012)" from Liaoning Province, Grant/Award Number: 88030312004

Abstract

Myeloid-derived suppressor cells (MDSCs) are responsible for antitumor immunodeficiency in tumor-bearing hosts. Primarily, MDSCs are classified into 2 groups: monocytic (M)-MDSCs and polymorphonuclear (PMN)-MDSCs. In most cancers, PMN-MDSCs (CD11b⁺Ly6C^{low}Ly6G⁺ cells) represent the most abundant MDSC subpopulation. However, the functional and phenotypic heterogeneities of PMN-MDSC remain elusive, which delays clinical therapeutic targeting decisions. In the 4T1 murine tumor model, CD11b⁺Ly6G^{low} PMN-MDSCs were sensitive to surgical and pharmacological interventions. By comprehensively analyzing 64 myeloid cell-related surface molecule expression profiles, cell density, nuclear morphology, and immunosuppressive activity, the PMN-MDSC population was further classified as CD11b⁺Ly6G^{low}CD205⁺ and CD11b⁺Ly6G^{high}TLR2⁺ subpopulations. The dichotomy of PMN-MDSCs based on CD205 and TLR2 is observed in 4T07 murine tumor models (but not in EMT6). Furthermore, CD11b⁺Ly6G^{low}CD205⁺ cells massively accumulated at the spleen and liver of tumor-bearing mice, and their abundance correlated with in situ tumor burdens (with or without intervention). Moreover, we demonstrated that CD11b⁺Ly6G^{low}CD205⁺ cells were sensitive to glucose deficiency and 2-deoxy-D-glucose (2DG) treatment. Glucose transporter 3 (GLUT3) knockdown by siRNA significantly triggered apoptosis and reduced glucose uptake in CD11b⁺Ly6G^{low}CD205⁺ cells, demonstrating the dependence of CD205⁺ PMN-MDSCs survival on both glucose uptake and GLUT3 overexpression. As GLUT3 has been recognized as a target for the rescue of host antitumor immunity, our results further directed the PMN-MDSC subsets into the CD205⁺GLUT3⁺ subpopulation as future targeting therapy.

KEYWORDS

CD205, GLUT3, glycolysis, heterogeneity, PMN-MDSC

Chenghao Fu and Zhonglin Fu contributed equally to this work.

Shiliang Ma Lead Contact.

This is an open access article under the terms of the Creative Commons Attribution-NonCommercial-NoDerivs License, which permits use and distribution in any medium, provided the original work is properly cited, the use is non-commercial and no modifications or adaptations are made.

© 2020 The Authors. *Cancer Science* published by John Wiley & Sons Australia, Ltd on behalf of Japanese Cancer Association.

1 | INTRODUCTION

Myeloid-derived suppressor cells (MDSCs) are vital constituents of the immunosuppressive network that inhibit antitumor immunity and facilitate tumor progression.¹ The characteristics of MDSCs have been extensively examined since the 1970s, when these cells were first reported.² Cancer-induced MDSCs are subdivided into subpopulations of monocytic (M)-MDSC and polymorphonuclear (PMN)-MDSC.^{1,3} Unlike M-MDSC, however, the PMN-MDSC subpopulation remains poorly understood.^{4,5} PMN-MDSCs may, in fact, be pathologically activated neutrophils.⁶ In murine tumor models, PMN-MDSCs and neutrophils share the same CD11b⁺Ly6C^{low}Ly6G⁺ cell surface markers, and protumor and antitumor functions have been reported for these cells.^{4,7} Therefore, not all tumor-induced PMN-MDSCs are disadvantageous to tumor progression, and it is informative to elucidate the cellular heterogeneity of the PMN-MDSC subpopulation.

It was proposed that PMN-MDSCs, rather than neutrophils, exhibit immunosuppression activity. PMN-MDSCs exhibit molecular and biochemical characteristics distinct from those of neutrophils. Unlike neutrophils, PMN-MDSCs lose much of their phagocytic capacity at maturity and are virtually undetectable in healthy individuals.⁴ A loss of cell density is associated with PMN-MDSC immunosuppressive function.⁸ Another study demonstrated that, in density-enriched PMN-MDSCs, upregulated lectin-type oxidized low-density lipoprotein (LDL) receptor 1⁺ (LOX-1⁺) rather than LOX-1⁻ cell subsets have immunosuppression activity.⁹ These results suggested that immunosuppression activity is determined by multiple factors.

Energy metabolism reprogramming is characteristic of tumor and other rapidly proliferating cells.^{10,11} A recent study showed that aerobic glycolysis controls MDSC accumulation and immunosuppression in triple-negative breast cancer via a specific CCAAT/enhancer-binding protein beta (CEBPB) isoform.¹² Enhanced glucose metabolism may be associated with MDSC survival,¹³ and fatty acid transport protein 2 upregulation mediates PMN-MDSC immunosuppression.¹⁴ Hence, membrane transporters are vital in MDSC biology. Glucose transporters (GLUTs) control glucose homeostasis.¹⁵ However, the relationship between GLUTs and MDSC accumulation remains unclear.

Here, we observed that various PMN-MDSC subpopulations differed in terms of their responses to alterations in the 4T1 tumor burden. We measured the expression levels of 64 clusters of differentiation (CD) molecules in different PMN-MDSC subpopulations and found that CD205 and TLR2 distinguished PMN-MDSC subpopulations. The 2 PMN-MDSC subpopulations have different immunosuppression activity levels. Under various tumor burden conditions, the infiltration patterns of these PMN-MDSCs differ significantly. We also demonstrated that they differed markedly in terms of their relative sensitivity to glucose deprivation and established that GLUT3 plays an important role in PMN-MDSC glucose absorption and survival. Our results suggest that glucose metabolism patterns affect PMN-MDSC immunosuppression. This study

also proposes therapeutic targets for the elimination of MDSC populations.

2 | MATERIALS AND METHODS

2.1 | Mice, cell line, and tumor model

Female BALB/c mice aged 6–8 wk were purchased from the Changsheng Animal Resources Center (Benxi, Liaoning, China). All procedures were conducted in accordance with the Animal Husbandry Guidelines of Shenyang Agricultural University. The Ethical Committee of Shenyang Agricultural University approved the study (Permit No. SYXK < Liao >2011-0001).

The 4T1 cell line of mouse breast carcinoma was obtained from the Cell Bank of the Chinese Academy of Sciences (Shanghai, China). The cells were maintained in RPMI 1640 medium (HyClone™; GE Healthcare, Chicago, IL, USA), supplemented with 10% (v/v) fetal bovine serum (FBS; Gibco, Grand Island, NY, USA), 2 mmol/L glutamine, 100 µg mL⁻¹ penicillin, and 100 µg mL⁻¹ streptomycin (Gibco, Grand Island, NY, USA).

A density of 2×10^5 4T1 cells in 100 µL RPMI 1640 medium was transplanted into the right fourth mammary gland. The tumor volume was calculated as follows¹⁶: $[L \times W^2]/2$

where L = tumor length and W = tumor width.

2.2 | Antibody staining and flow cytometry

Tumor and lung samples were minced and digested with a mixture of 2 mg mL⁻¹ collagenase, 2 mg mL⁻¹ hyaluronidase, and 1 mg mL⁻¹ DNase (Sigma-Aldrich Corp., St. Louis, MO, USA) in phosphate-buffered saline (PBS) at 37°C for 60 min. All other tissues were passed through a 70 µm nylon mesh after homogenization in RPMI 1640 medium. Erythrocytes (RBCs) were depleted with ACK Lysing Buffer (Thermo Fisher Scientific).¹⁷ Single-cell suspensions were incubated with anti-mouse CD16/32 antibody (BioLegend, San Diego, CA, USA) to avoid nonspecific antibody binding via Fc receptors. Cells were then stained with fluorescence-conjugated antibodies in accordance with the manufacturer's recommendations.

Unless otherwise stated, a combination of fixable viability dye eFluor-455UV (FVD455)/7-AAD, anti-CD45-APC-Cy7, anti-CD11b-APC/PE, anti-Ly6G-PerCP-eFluor-710/FITC, anti-CD205-PE/Super bright-436, and anti-TLR2-FITC was used for recognizing immune cells.

Flow cytometry was performed using a FACS Fortessa or FACSAria III and FACSDiva software (BD Biosciences, San Jose, CA, USA) and analyzed with FlowJo v.10 (BD Biosciences, San Jose, CA, USA). For all flow cytometry assays, background and positive staining were distinguished via isotype and fluorescence minus 1 (FMO) controls. Circled or boxed populations were designated as positive relative to the isotype and FMO controls.

2.3 | In vivo chemotherapy drug treatment

Tumor-bearing mice were treated with doxorubicin (15 mg kg⁻¹; Sigma-Aldrich Corp., St. Louis, MO, USA), cyclophosphamide (100 mg kg⁻¹; Sigma-Aldrich Corp., St. Louis, MO, USA), and docetaxel (15 mg kg⁻¹; Sigma-Aldrich Corp., St. Louis, MO, USA) via intraperitoneal injection. The control mice were treated with PBS.

2.4 | MDSC and T-cell isolation and in vitro culture

CD205⁺ or TLR2⁺ PM subpopulations from the spleens of tumor-bearing mice were sorted using a FACSAria III instrument. Tumor-bearing mice were sacrificed 3 wk after 4T1 tumor cell transplantation. Their spleens were excised, homogenized in RPMI 1640 medium, and passed through a 70- μ m nylon mesh to generate single-cell suspensions. Anti-Ly6G-Percp cy5.5, anti-CD11b-APC, and propidium iodide (PI) stains were applied in accordance with the manufacturer's recommendations. A FACSAria III cell sorter with FACSDiva software (BD Biosciences, San Jose, CA, USA) was used to sort cell populations. The sorted cells were collected in complete medium (10% (v/v) FBS in RPMI 1640) for subsequent use in functional assays and adoptive transfer experiments.

T cells were separated by FACS or a CD8⁺ T-cell-negative isolation kit (MACS; Miltenyi Biotec, Bergisch Gladbach, Germany) in accordance with the manufacturer's instructions. Tumor-free splenocytes were incubated with a cocktail of biotin-conjugated antibodies against CD4, CD11b, CD11c, CD19, CD45R (B220), CD49b (DX5), CD105, anti-MHC-class II, Ter-119, and TCR γ/δ . The isolation of T cells was achieved by depletion of magnetically labeled cells. Sorted populations were collected in complete medium (10% (v/v) FBS in RPMI 1640) for subsequent use in functional assays.

2.5 | In vitro T-cell suppression assay

T-cell proliferation was determined from the changes in fluorescence intensity via a carboxyfluorescein succinimidyl ester (CFSE) kit (BioLegend, San Diego, CA, USA). Splenocytes were suspended in serum-free RPMI 1640, incubated with 2.5 mmol/L CFSE at 20°C for 10 min, washed 3 times with a 5-fold volume of complete medium (RPMI 1640 containing 10% (v/v) FBS), and washed once with cold PBS. The CFSE-labeled T cells were then stimulated with anti-CD3/CD28 antibody (eBioscience, San Diego, CA, USA), and an equal number of MDSCs was added to a round-bottomed 96-well plate at various ratios. After 72 h of incubation, the cells were harvested and labeled with fluorescence-conjugated antibodies. The CFSE signals of the gated lymphocytes were analyzed using the FACS AriaIII instrument (BD Bioscience, San Jose, CA, USA). Cell proliferation was quantified using FlowJo v.10 software (BD Bioscience, San Jose, CA, USA).

2.6 | 2-NBDG uptake assay

Cells were plated at a density of 1×10^6 well⁻¹ in 24-well plates and suspended in glucose-free Dulbecco's modified Eagle's medium (DMEM; Gibco, Grand Island, NY, USA) containing 100 μ mol/L 2-NBDG (BioLegend, San Diego, CA, USA). After incubation at 37°C under 5% CO₂ in air for 30 min, the medium was replaced with fresh DMEM and the incubation continued for another 5 min. The cells were washed twice with PBS before flow cytometry analysis.

2.7 | Apoptosis assay

Apoptotic cells were detected using a Pacific Blue Annexin V apoptosis detection kit (BioLegend, San Diego, CA, USA) followed by surface marker staining and flow cytometry analysis. Early apoptotic cells were defined as annexin V-positive and PI/7-AAD-negative. Late apoptotic cells were designated annexin V-positive and PI/7-AAD-positive.

2.8 | Adoptive transfer

CD205⁺ PMN-MDSC or TLR2⁺ PMN-MDSC subpopulations from the spleens of tumor-bearing mice were sorted on a FACSAria III instrument, subjected to flow cytometry to confirm > 95% purity, adjusted to 5×10^8 mL⁻¹ in 200 μ L RPMI 1640, and intravenously injected into tumor-bearing mice. The mice received sorted cells every 4 d for a total of 3 treatments.

2.9 | In vivo intermittent fasting treatment

Animals underwent complete food deprivation with access to water for 48–60 h to attain a 20% body weight loss. During the fasting period, mice were individually housed in clean, new cages to reduce cannibalism, coprophagy, and residual chow. Body weight and blood glucose levels were measured immediately before, during, and after fasting.

2.10 | siRNA

GLUT3 mRNA was knocked down via a GLUT3-siRNA assay (Invitrogen, Carlsbad, CA, USA) in accordance with the manufacturer's recommendations. Lipofectamine[®] 3000 reagent was combined with the siRNAs or negative control siRNA in Opt-MEM medium and the mixtures were added to 24-well plates. The siRNA knockdown efficiency was evaluated using immunoblotting or real-time RT-qPCR.

2.11 | Western blot

Total protein was extracted from various tissues or sorted cells and the supernatant protein concentrations were determined using the

bicinchoninic acid (BCA) assay (Beyotime, Jiangsu, China). Equal amounts of protein were separated on sodium dodecyl sulfate-polyacrylamide (SDS-PAGE) gels and transferred to polyvinylidene fluoride (PVDF) membranes (Millipore, Bedford, MA, USA) via a wet trans blot system. The membranes were then blocked with 5% (w/v) nonfat dried milk for 1 h at 25°C, incubated with anti-GLUT1, anti-GLUT3, anti-PARP, anti-caspase 3, or anti- β -actin antibodies (EnoGene, Nanjing, China) at 4°C overnight, and incubated with horseradish peroxidase-conjugated secondary antibody at room temperature for 1 h. The blots were visualized with an enhanced chemiluminescence (ECL) kit (Beyotime, Jiangsu, China).

2.12 | Quantitative real-time PCR

Total RNA was isolated with TRIzol[®] reagent (Invitrogen, Carlsbad, CA, USA) in accordance with the manufacturer's instructions and reverse transcribed into cDNA using a RevertAid First Strand cDNA synthesis kit (Invitrogen, Carlsbad, CA, USA). A KAPA SYBR FAST qPCR kit (Kapa Biosystems Inc, Wilmington, MA, USA) and the corresponding primer sets (Table S1) were used for RT-qPCR in a Bio-Rad CFX96 real-time system (Bio-Rad Laboratories, Hercules, CA, USA). Relative expression was normalized to β -actin and calculated using the $2^{-\Delta\Delta Ct}$ method.

2.13 | Statistical analysis

Unless otherwise stated, all experiments were repeated at least 3 times. Only representative data are shown. Statistical analyses were performed using GraphPad Prism v.6 (GraphPad Software, Inc, La Jolla, CA, USA) and Microsoft[®] Excel 2016 (Microsoft Corporation, Redmond, WA, USA).

Flow cytometry plots showed representative examples of the relative percentages of each population or subpopulation. To obtain the absolute or calculated percentage of a particular subpopulation, its relative percentage was multiplied by the relative percentage of its parent population and the product was divided by 100 and presented as an absolute percentage.

One-way ANOVA or Student *t* tests were performed to determine whether treatment means differed significantly. The output was then subjected to Bonferroni multiple group comparisons or Fisher least significant difference (LSD) post-test. Unless otherwise indicated, significance was as follows: ****P* < .001, ***P* < .01, and **P* < .05.

3 | RESULTS

3.1 | Accumulation level of CD11b⁺Ly6G^{low} cells is sensitive to tumor burden

Sufficient evidence indicates that neutrophils have antitumor activity,^{18,19} whereas cells are defined as PMN-MDSC on the basis of

the potent immunosuppressive activity in tumor-bearing hosts.¹ It is now accepted that PMN-MDSC accumulate at various degrees and co-exist with neutrophils in tumor-bearing hosts.⁶ However, the unavailability of reliable markers to recognize immunosuppressive subsets of tumor-derived CD11b⁺Ly6G⁺ cells has delayed its decision as a clinical therapeutic target.

CD11b⁺Ly6G⁺ represents the minimum phenotypic characteristics required to identify PMN-MDSCs and neutrophils.¹ Thus, we recognized the presence of CD11b⁺Ly6G⁺ cells in both tumor-free and tumor-bearing mice (Figure S1A, B). The results show that 4T1 tumor transplantation substantially increased CD11b⁺Ly6G⁺ cell accumulation in all organ compartments (Figure S1B). The accumulation of polymorphonuclear granulocytes in the spleen and liver was confirmed by hematoxylin-eosin staining. Interestingly, we observed that, compared with CD11b⁺Ly6G⁺ cells in tumor-free mice, tumor-induced CD11b⁺Ly6G⁺ cells expressed a lower level of Ly6G molecule and had a lower side scatter (Figure S1C). In addition, >70% of CD11b⁺Ly6G⁺ cells were located in the CD11b⁺Ly6G^{high} areas in tumor-free mice (marked by blue lines in Figure 1A). While 60% of tumor-induced CD11b⁺Ly6G⁺ cells were in the CD11b⁺Ly6G^{low} areas (marked by red lines in Figure 1A). Furthermore, tumor-induced CD11b⁺Ly6G^{low} cells decreased sharply when in situ tumors were resected or attenuated via chemotherapy. In contrast, there was no significant alteration in CD11b⁺Ly6G^{high} cells (Figure 1B, C). The variation of the Ly6G^{high} to Ly6G^{low} ratio in the tumor-free or tumor-bearing mice strengthens the conclusion that CD11b⁺Ly6G^{high} and CD11b⁺Ly6G^{low} cells responded heterogeneously to the tumor burden (Figure 1D).

3.2 | CD molecule expression profiles of various CD11b⁺Ly6G⁺ cell subpopulations

To further identify the differences among CD11b⁺Ly6G⁺ cell subpopulations, a four-color flow cytometry (FCM) was performed using 64 immune cell CD molecules including chemokine receptors (CCRs) and interleukin receptors (ILRs). We found that compared with the CD11b⁺Ly6G^{low}Ly6G⁺ cells in tumor-free mice, >40% of the CD molecular expression levels in cells with the same phenotype showed significant changes in the 4T1 tumor mice (Figure S2A). Furthermore, CD11b⁺TLR2⁺ cells expressed a higher level of Ly6G molecules than CD11b⁺CD205⁺ cells in tumor-bearing mice (Figure S2B).

No previous reports of differences existed between these CD11b⁺Ly6G⁺ subpopulations in terms of their CD205 or TLR2 expression levels. Therefore, we characterized the levels of the 64 CD molecules expressed by the CD11b⁺Ly6G^{high} cells, CD11b⁺Ly6G^{low} cells, CD11b⁺Ly6G⁺CD205⁺ cells, and CD11b⁺Ly6G⁺TLR2⁺ cells. The expression traits of CD11b⁺Ly6G^{low} cells most closely resembled those of the subpopulation represented by CD11b⁺Ly6G⁺CD205⁺. Compared with the abundant CD molecules, such as CXCR2 and B7-H1, expressed by the CD11b⁺Ly6G⁺TLR2⁺ and CD11b⁺Ly6G^{high} subpopulations, the CD11b⁺Ly6G⁺CD202⁺ subpopulation showed

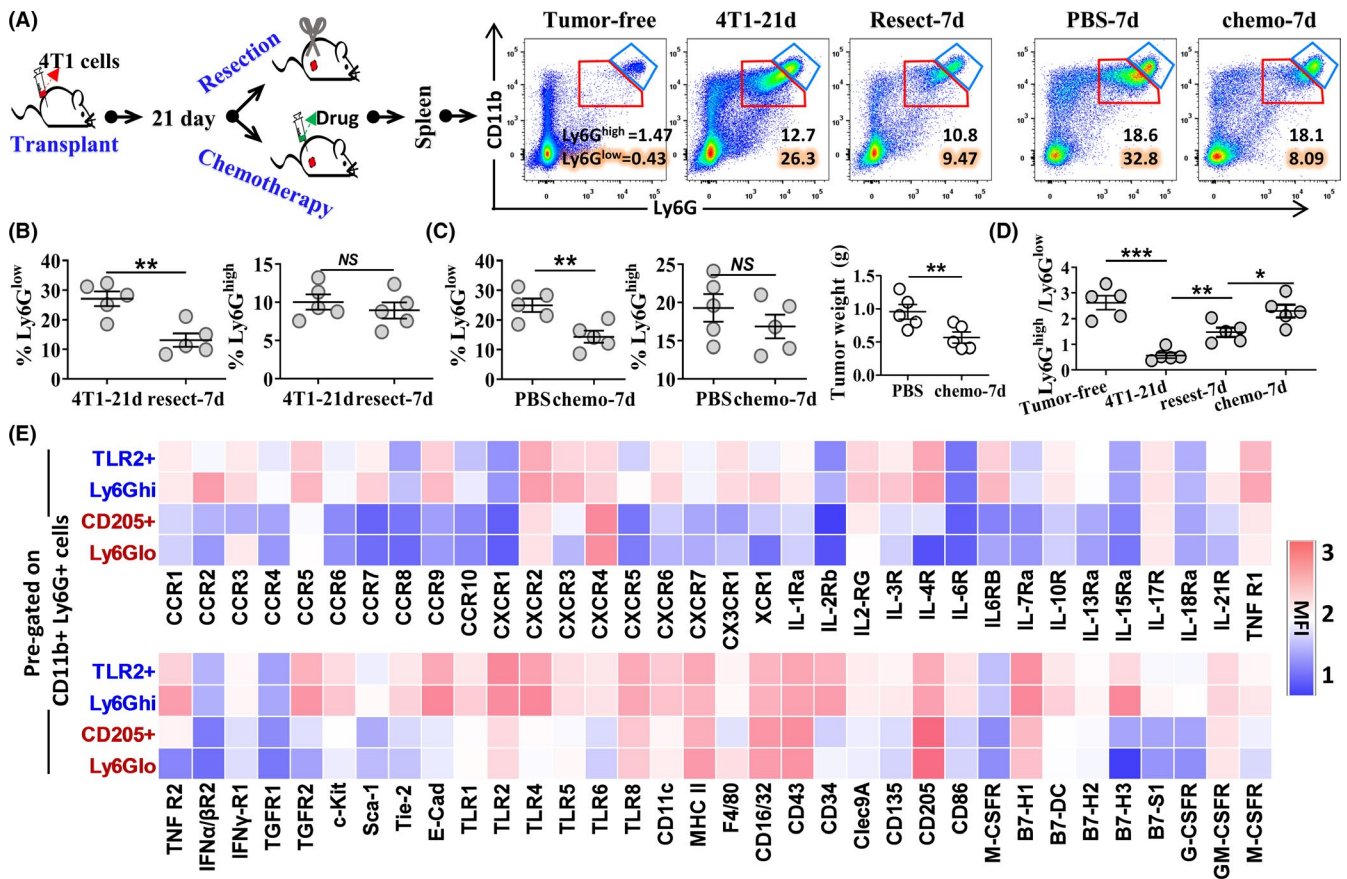


FIGURE 1 CD11b⁺Ly6G^{low} cells differ from CD11b⁺Ly6G^{high} cells in frequency and CD protein expression profile. A–D, Mice were subcutaneously inoculated with or without 2×10^5 4T1 cells. Surgical resection of the tumor was performed, and chemotherapy was administered 3 wk after 4T1 cell inoculation, and splenic leukocytes were collected and analyzed by flow cytometry (FCM) at the indicated time points (in days). A, FCM pseudo-color plots display the proportion of CD11b⁺Ly6G^{high} and CD11b⁺Ly6G^{low} cell subsets. The gating reference for Ly6G^{high} subsets was based on the main CD11b⁺Ly6G^{high} population identified in tumor-free mice. B, C, Percentage of splenic CD11b⁺Ly6G^{high} and CD11b⁺Ly6G^{low} subsets upon 7 d of the indicated treatments. D, CD11b⁺Ly6G^{high}/CD11b⁺Ly6G^{low} ratio under the indicated conditions. E, Mice were subcutaneously inoculated with or without 2×10^5 4T1 cells and euthanized after 3 wk. Splenic cells collected from tumor-bearing mice were evaluated by FCM. Heatmap shows the mean fluorescence intensity (MFI) of the indicated molecules on the CD11b⁺Ly6G⁺ subpopulation. Ly6G^{lo/hi} represents CD11b⁺Ly6G^{low/high} cells, TLR2⁺ represents CD11b⁺Ly6G^{high}TLR2⁺ cells, and CD205⁺ represents CD11b⁺Ly6G^{low}CD205⁺ cells. Data represent ≥ 3 independent experiments and are shown as means \pm standard deviation. * $P < .05$, ** $P < .01$, *** $P < .001$, ns = significant, by Student t test

high expression of CXCR4, CD16/CD32, CD43, and CD205 only (Figure 1E).

3.3 | CD11b⁺Ly6G⁺ cells can be classed into CD205⁺ and TLR2⁺ subpopulations in 4T1 and 4T07 murine tumor models (but not in EMT6)

In mice, the CD11b⁺Gr-1⁺ phenotype comprises all MDSCs; in addition, Ly6G expression serves to further classify MDSCs into PMN-MDSC (CD11b⁺Ly6G^{low}Ly6G⁺) or M-MDSC (CD11b⁺Ly6G^{high}Ly6G⁻).¹ However, to better characterize the MDSC subpopulations, we established a back-gating view of multicolor FCM data. We set the M-MDSC, PMN-MDSC, CD205⁺ PMN-MDSC, and TLR2⁺ PMN-MDSC subsets as purple, red, blue, and yellow dot plots, respectively.

We observed that the M-MDSC phenotype was CD11b⁺Gr-1^{low}Ly6G^{high}Ly6G⁻ and that of PMN-MDSC was CD11b⁺Gr-1^{high}Ly6G^{low}Ly6G⁺ (Figure 2A). We concluded that PMN-MDSC could be further characterized by CD205⁺ and TLR2⁺ subsets. The CD205⁺ PMN-MDSC and TLR2⁺ subset phenotypes comprised CD11b⁺Ly6G^{low}Gr-1^{low}Ly6G^{low} and CD11b⁺Ly6G^{low}Gr-1^{high}Ly6G^{hi}, respectively (Figure 2A). When we gated the CD11b⁺Ly6G⁺ subsets, CD11b⁺Ly6G⁻Ly6G^{high} cells (M-MDSC) were excluded. Thus, anti-Ly6C and anti-Gr-1 antibodies were not required to identify CD205⁺ PMN-MDSC and TLR2⁺ PMN-MDSC in the 4T1 tumor model (Figure 2B). Moreover, anti-Gr-1 mAb (clone: RB6-8C5) was used to eliminate MDSCs in tumor models,²⁰ indicating that anti-Gr-1 mAb did impact the physiological activity of the MDSCs. To avoid introducing unnecessary external signals to MDSCs, we employed minimal phenotypic characteristics to identify the MDSC and its subpopulations.

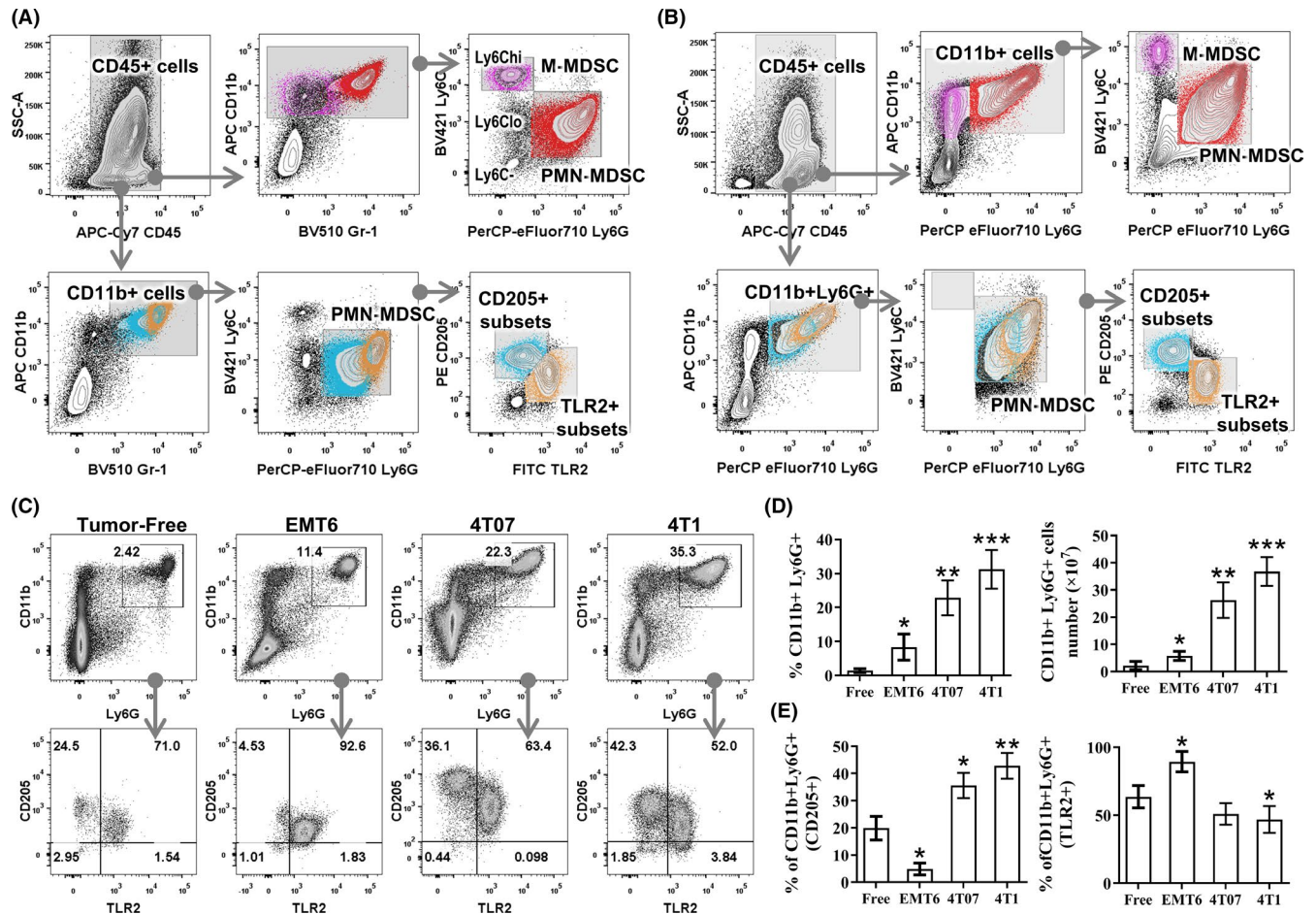


FIGURE 2 A dichotomy of polymorphonuclear myeloid-derived suppressor cells (PMN-MDSCs) based on CD205 and TLR2 expression. Mice were subcutaneously inoculated with or without 2×10^5 4T1 cells and euthanized after 3 wk. Splenic cells were collected from tumor-bearing mice, and immune cell populations were detected by flow cytometry (FCM). A, B, Representation of the FCM back-gating strategy applied to 2 independent staining experiments for identification of MDSC subpopulation. A, Fixable viability dye eFluor 455UV (FVD455), anti-CD45-APC-Cy7, anti-CD11b-APC, anti-Ly6G-PerCP-eFluor710, anti-Ly6C-BV421, anti-CD205-PE, anti-TLR2-FITC, and anti-Gr-1-BV510 antibodies were used. B, The same antibodies as in (A) were used, except anti-Gr-1-BV510, which was abandoned. C-E, Mice were subcutaneously inoculated with or without 2×10^5 4T1, EMT6, or 4T07 cells and euthanized after 3 wk. Splenic cells collected from tumor-bearing and tumor-free mice were detected by FCM. C, FCM pseudo-color plots display the proportion of various CD11b⁺Ly6G⁺ subpopulations. D, Proportion and number of CD11b⁺Ly6G⁺ cells. E, Ratio of TLR2⁺ or CD205⁺ subsets within total CD11b⁺Ly6G⁺ cells. Data represent ≥ 3 independent experiments and are shown as means \pm standard deviation. Data were analyzed * $P < .05$, ** $P < .01$, *** $P < .001$, ns = significant, by Student t test

Many researchers have reported that MDSCs constitute a heterogeneous cell population. Therefore, we constructed 3 murine breast tumor models (4T1, 4T07, and EMT6) to confirm if the same phenomenon occurred in other cell lines. In the 4T1 and 4T07 tumor-bearing mice, we observed that total CD11b⁺Ly6G⁺ cell numbers in the spleen increased by 15-fold compared with that of tumor-free mice. Furthermore, PMN-MDSCs comprised CD205⁺ and TLR2⁺ subpopulations, and $<5\%$ of CD11b⁺Ly6G⁺ cells were CD205⁺ TLR2⁻ (Figure 2C, D). The relative proportions of CD205⁺ subsets within CD11b⁺Ly6G⁺ cells increased from 19.9 ± 4.6 (in tumor-free mice; Figure 2E) to 35.5 ± 3.7 (in 4T07 mice) and 41.0 ± 6.3 (in 4T1 mice). However, in the EMT6 murine tumor model, $>90\%$ of CD11b⁺Ly6G⁺ cells were TLR2⁺ subsets. Therefore, in the 4T1 and 4T07 murine tumor models (but not in EMT6), PMN-MDSCs consisted of CD205⁺ and TLR2⁺ subpopulations.

3.4 | CD11b⁺Ly6G^{low}CD205⁺ cells strongly suppress CD8⁺ T-cell antitumor response activity

To determine the relationship between CD11b⁺Ly6G^{low}CD205⁺ cells and antitumor immunity, we established a tumor graft rejection model. After resection of the first transplanted tumor, mice reject the re-transplanted tumor cells.²¹ This response was mainly mediated by CD8⁺ T cells.²² Here, we repeated tumor graft rejection in the 4T1 tumor model (Figure 3A) and sorted the CD8⁺ T cells using magnetic beads. Sorted CD8⁺ T cells derived from mice receiving re-transplanted 4T1 cells are, from this point forwards, primed-CD8⁺ T cells. To reduce the disturbance of antibodies on MDSC or the immune system, only indicated antibodies were used. The sorted cells were checked using flow cytometry, and

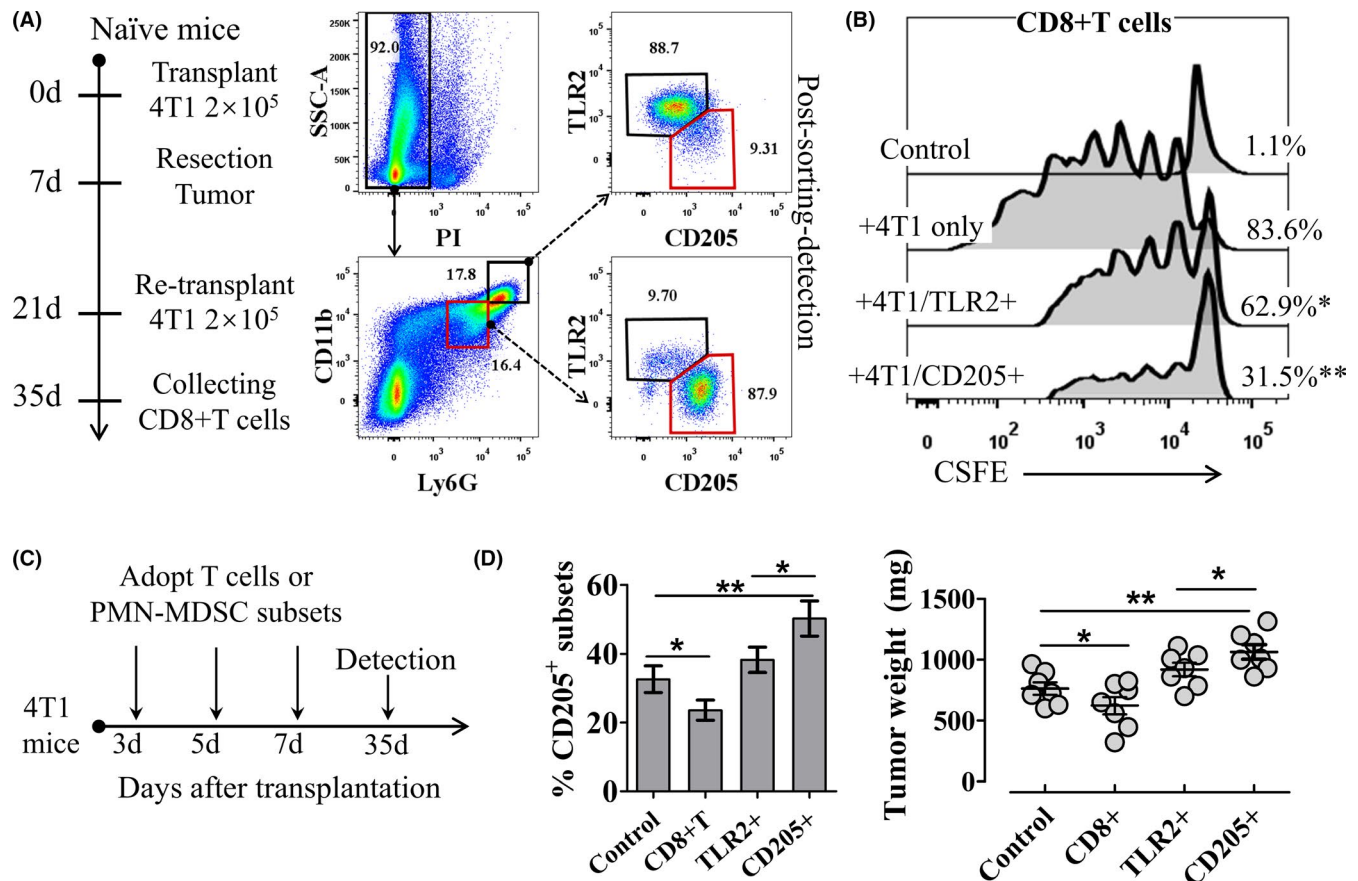


FIGURE 3 CD11b⁺Ly6G^{low}CD205⁺ cells potently suppress the CD8⁺ T-cell antitumor response. A, Mice were subcutaneously inoculated with 2×10^5 4T1 cells, and in situ tumor was surgically resected after 7 d. Re-implantation of 2×10^5 4T1 cells was performed on day 14 after the initial resection. CD8⁺ T cells were then collected 14 d after the new inoculation. CD11b⁺Ly6G^{high}TLR2⁺ cells and CD11b⁺Ly6G^{low}CD205⁺ cells were sorted by FCM from tumor-bearing mice. B, Sorted CD8⁺ T cells in (A) acted as responder cells, whereas 4T1 cells mixed with or without CD11b⁺Ly6G⁺ subpopulations acted as stimulator cells. The proliferation status of CD8⁺ T-responder cells was evaluated by CFSE dilution. C, D, Mice were subcutaneously inoculated with 2×10^5 4T1 cells and received sorted CD11b⁺Ly6G^{high}TLR2⁺ cells and CD11b⁺Ly6G^{low}CD205⁺ cells on days 3, 5, and 7 post-transplantation. C, Schematic diagram of the adoptive transfer assays. D, CD11b⁺Ly6G^{low}CD205⁺ cell proportion and in situ tumor weight in tumor-bearing mice. Tumor-bearing mice received PBS, sorted CD8⁺ T cells, CD11b⁺Ly6G^{high}TLR2⁺ cells, or CD11b⁺Ly6G^{low}CD205⁺ cells, indicated as control, CD8⁺ T, TLR2⁺, or CD205⁺, respectively. Data represent ≥ 3 independent experiments and are shown as means \pm standard deviation. * $P < .05$, ** $P < .01$, *** $P < .001$, ns = significant as determined by one-way ANOVA and Tukey's post-tests

>85% purity was obtained (Figure 3A). CFSE-labeled primed-CD8⁺ T cells were cultured either alone or along with 4T1 cells, and the former proliferated in the mixed culture only. However, CD8⁺ T-cell proliferation was significantly inhibited by the addition of the CD11b⁺Ly6G⁺ subpopulation to the mixed culture system. Furthermore, the inhibition rate of CD11b⁺Ly6G^{low}CD205⁺ cells was significantly higher than that of CD11b⁺Ly6G^{high}TLR2⁺ cells (Figure 3B).

We performed an adoptive transfer assay on primed-CD8⁺ T cells and the CD11b⁺Ly6G⁺ subpopulation (Figure 3C). Tumor weights and splenic CD205⁺CD11b⁺Ly6G^{low} cell levels were significantly lower in the primed-CD8⁺ T-cell recipient mice than they were in the control groups. In contrast, mice receiving the CD11b⁺Ly6G^{low}CD205⁺ subpopulation presented with higher splenic CD11b⁺Ly6G^{low}CD205⁺ cell levels and tumor weights compared with the control groups. The CD11b⁺Ly6G^{low}CD205⁺ cell recipients had the greatest tumor

weights (Figure 3D). Therefore, CD11b⁺Ly6G^{low}CD205⁺ cells potently suppressed antitumor immunity.

3.5 | CD11b⁺Ly6G⁺ subpopulations represented by CD205 and TLR2 are morphologically and phenotypically heterogeneous

We then investigated whether the accumulation of CD11b⁺Ly6G^{low}CD205⁺ cells was organ dependent (Figure 4A). Most of the CD11b⁺Ly6G^{low}CD205⁺ cells in the tumor-free mice were localized to the bone marrow. A substantial concentration was seen in the spleen compartment, unlike in the peripheral circulation, where only trace amounts were found. After 4T1 tumor transplantation, the levels of CD11b⁺Ly6G^{low}CD205⁺ cells in the peripheral circulation were significantly increased and these cells

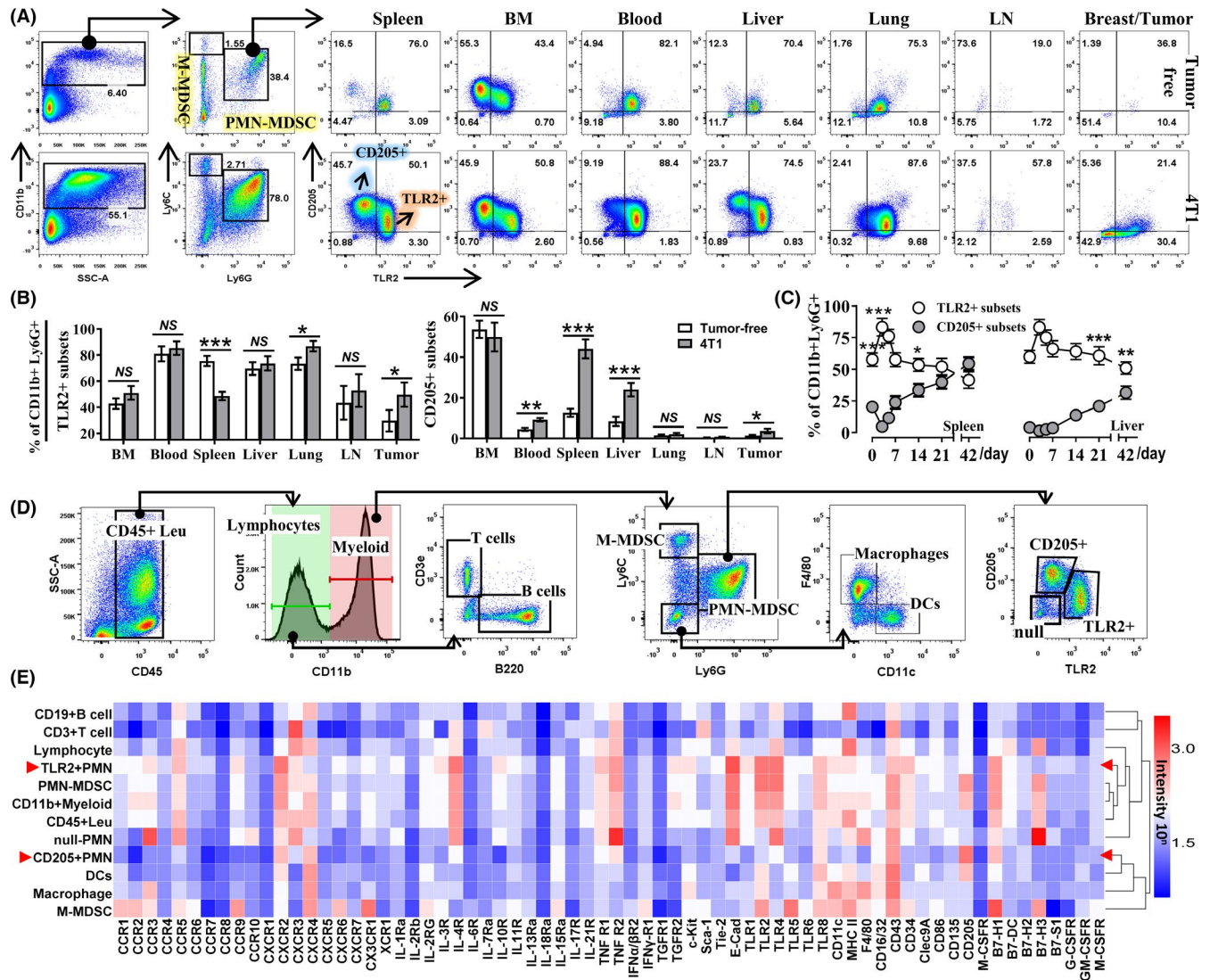


FIGURE 4 CD11b⁺Ly6G⁺ subpopulations represented by CD205 and TLR2 are morphologically and phenotypically heterogeneous. Mice were subcutaneously inoculated with or without 2×10^5 4T1 cells and euthanized after 3 wk. Leukocytes from various organs of tumor-bearing and tumor-free mice were detected by flow cytometry (FCM). A, FCM pseudo-color plots display the proportion of CD11b⁺Ly6G^{low}CD205⁺ cells and CD11b⁺Ly6G^{high}TLR2⁺ cells. B, Proportion of CD11b⁺Ly6G⁺ subpopulations in indicated organs of tumor-free and tumor-bearing mice. C, Proportion of CD11b⁺Ly6G^{low}CD205⁺ cells and CD11b⁺Ly6G^{high}TLR2⁺ cells in the spleen and liver of tumor-bearing mice. D, FCM gate strategy for splenic leukocytes from tumor-bearing mice. E, Heatmap showing the expression profile of CCR1 (or other exhibited molecules) in various leukocyte subpopulations of tumor-bearing mice. Data represent ≥ 3 independent experiments and are shown as means \pm standard deviation. * $P < .05$, ** $P < .01$, *** $P < .001$, ns = significant, as determined by Student *t* test

were localized mostly to the liver and spleen (Figure 4B). Therefore, peripheral accumulation of CD11b⁺Ly6G^{low}CD205⁺ cells is organ dependent.

Cluster analysis of the CCRs and Toll-like receptors (TLRs) expressed by the CD11b⁺Ly6G⁺ cell subpopulation in the bone marrow, peripheral blood, spleen, liver, and lung compartments revealed that CD11b⁺Ly6G^{low}CD205⁺ cell accumulation in the spleen and liver was consistent with CXCR4 expression. Hence, the CXCR4/CCL12 axis may mediate organ-dependent accumulation of these cells (Figure S3A).

Accumulation rates of the 2 CD11b⁺Ly6G⁺ cell subpopulations in the spleen compartment changed during transplanted tumor growth. TLR2⁺ subsets rapidly accumulated in the first week after

transplantation, whereas CD205⁺ subsets rapidly accumulated later (Figure 4C).

To determine whether the CD11b⁺Ly6G^{low}CD205⁺ cells possessed other CD molecules that distinguished them from other leukocytes, we used a multicolor FCM staining strategy to establish the CD expression profiles of the splenic leukocytes (Figure 4D, E). Cluster analysis disclosed that CD11b⁺Ly6G^{low}CD205⁺ cells had a CD expression profile similar to that of DCs, but markedly different from those of lymphocytes and CD11b⁺Ly6G^{high}TLR2⁺ cells. Relative to CD11b⁺Ly6G^{high}TLR2⁺ cells, CD11b⁺Ly6G^{low}CD205⁺ cells had simpler nuclear morphology and lower cell density (Figure S3B-E). Therefore, the CD11b⁺Ly6G⁺ cell subpopulations represented by CD205 and TLR2 comprised comparatively independent myeloid cell subsets.

3.6 | Dynamic characteristics of CD11b⁺Ly6G^{low}CD205⁺ cells in resected and chemotherapeutically treated tumor-bearing mice

Certain studies have reported that the reduction of the overall tumor burden by resection or chemotherapy might reverse immunosuppression and improve immunotherapy efficacy.^{23,24} However, resection may increase the risks of recurrence and metastasis and chemotherapeutic agents are toxic to lymphocytes. Moreover, a reference for the immunotherapy intervention time node must be provided. Therefore, it is necessary to establish the dynamic characteristics of the alterations in the immune cell subsets in tumor-bearing hosts at various cancer stages.

Here, the 4T1 tumor resection model demonstrated that tumor recurrence rates increased with resection delay (Figure 5A). After in situ tumor removal, the CD11b⁺Ly6G⁺ cell levels decreased weekly until they became normalized (~3%) (Figure 5B). The TLR2⁺ subsets gated on CD11b⁺Ly6G⁺ cells declined to normal levels 1 wk after the in situ tumor removal. Nevertheless, the CD205⁺ subsets remained elevated for another week (Figure 5B, C). Along with the decreases in the CD11b⁺Ly6G^{low}CD205⁺ cells, the proportions of CD3e⁺CD4⁺, CD3e⁺CD8a⁺, and CD19⁺ were restored to normal levels 2 wk after primary tumor excision (Figure 5D). Therefore, the restoration of the lymphocyte ratio in tumor-bearing hosts is associated with the homeostasis of the CD11b⁺Ly6G⁺ cell subpopulation.

Mice with different tumor burdens simulating early, mid-advanced, and advanced cancer stages were administered chemotherapeutic agents (Figure 5E). Chemotherapy restricted in situ tumor size before the mass reached 2% of the body weight (Figure 5E). The proportions of CD11b⁺Ly6G⁺ cell subpopulations in the spleen were substantially reduced when the in situ tumor size was controlled (Figure 5F). Furthermore, the CD3⁺CD4⁺ and CD3⁺CD8⁺ T-lymphocyte levels significantly rebounded (Figure 5H). In contrast, when the in situ tumor size was left unregulated, the proportions of CD11b⁺Ly6G^{low}CD205⁺ cells increased to levels surpassing those of the non-chemotherapy-receiving group (Figure 5F) and TLR2⁺ subsets showed no uniform changes. For those reasons, the CD11b⁺Ly6G⁺CD205⁺ cells may be associated with in situ tumor growth after chemotherapy (Figure 5G).

The chemotherapy interventions also disrupted the immune system dramatically. The B lymphocyte levels decreased considerably after chemotherapeutic intervention and gradually recovered after that (Figure 5H). The ratio of CD205⁺ subsets to TLR2⁺ subsets was not normalized even 5 wk after chemotherapy intervention (Figure 5G). Hence, imbalances in the CD11b⁺Ly6G⁺ subpopulations are mainly determined by the tumor burden, and CD205⁺ subsets might be the main factor mediating T-lymphocyte immunodeficiency.

Overall, these data showed that the CD11b⁺Ly6G^{low}CD205⁺ cell rate in the spleen indicated tumor progression and CD8⁺ T-cell recovery upon intervention treatment in the 4T1 model.

3.7 | GLUT3 expression is directly correlated with increased glucose uptake in CD11b⁺Ly6G^{low}CD205⁺ cells

Spleen weight growth curves were similar for both 4T1 tumor-bearing mice and in situ tumors. MDSC accumulation dramatically increased the spleen weight.²⁵ MDSC meets the proliferation energy requirement via metabolic reprogramming¹² and nutrition transporters influence this process.¹⁴ GLUTs are the most common cellular glucose transporters. However, the relationship between GLUTs and MDSC is unclear. Compared with the organs of tumor-free mice, GLUT expression in the organs of tumor-bearing mice was highly variable (Figure 6A). Compared with the 4T1 cell line, 4 types of GLUTs were upregulated in the transplanted tumor tissue (Figure 6A). Hence, other cell types in the tumor microenvironment might have rich energy metabolism patterns. GLUT2 was significantly downregulated in most organs including the liver. GLUT1 and GLUT3 were upregulated in all organs except the lymph nodes (LN) (Figure 6A). These expression patterns coincided with MDSC accumulation patterns in the organs (Figures 1A and 6A). GLUT1 and GLUT3 expression increased with tumor burden (Figure 6B). Therefore, GLUT expression could be linked to CD11b⁺Ly6G⁺ cell accumulation.

We also measured the GLUT expression in splenic leukocyte subpopulations. Compared with lymphocytes, GLUT1 and GLUT3 were significantly upregulated in CD11b⁺Ly6G⁺ cells (Figure 6C). The CD11b⁺Ly6G^{low}CD205⁺ cells expressed the highest GLUT3 levels of all splenic immune cells (Figure 6D). GLUT1 and GLUT3 are high-affinity glucose transporters.¹⁵ We used the glucose fluorescence analog 2NBDG to compare the glucose transport rates among various immune cells (Figure 6E). The mean fluorescence intensity (MFI) of each splenic leukocyte subpopulation was consistent with the GLUT3 expression level after incubation with 2NBDG for 30 min (Figure 6E). After 120 min incubation with 2NBDG, however, MFI was similar for both CD11b⁺Ly6G⁺ cell subpopulations and was significantly higher compared with that of the CD3⁺ T cells (Figure 6E). Thus, GLUT3 may participate in the metabolic reprogramming of PMN-MDSC.

3.8 | Blocking glucose metabolism induces CD11b⁺Ly6G^{low}CD205⁺ cell apoptosis in vitro

As PMN-MDSCs have a short lifespan (<3 d),²⁶ we used interfering RNA technology to knock down GLUT3 expression and measure CD11b⁺Ly6G⁺ cell survival rate and glucose uptake.

The apoptosis rates of CD3⁺ T, CD205⁺, and TLR2⁺CD11b⁺Ly6G⁺ cells cultured under 2DG and glucose-free conditions were significantly higher than those under normal culture conditions. A dose-dependent relationship existed between apoptosis rate and 2DG or glucose uptake. However, the apoptosis rate of CD11b⁺Ly6G^{low}CD205⁺ cells was higher than that of TLR2⁺ subsets (Figure 7A). Glucose deficiency significantly upregulated GLUT3 in CD11b⁺Ly6G^{low}CD205⁺ cells

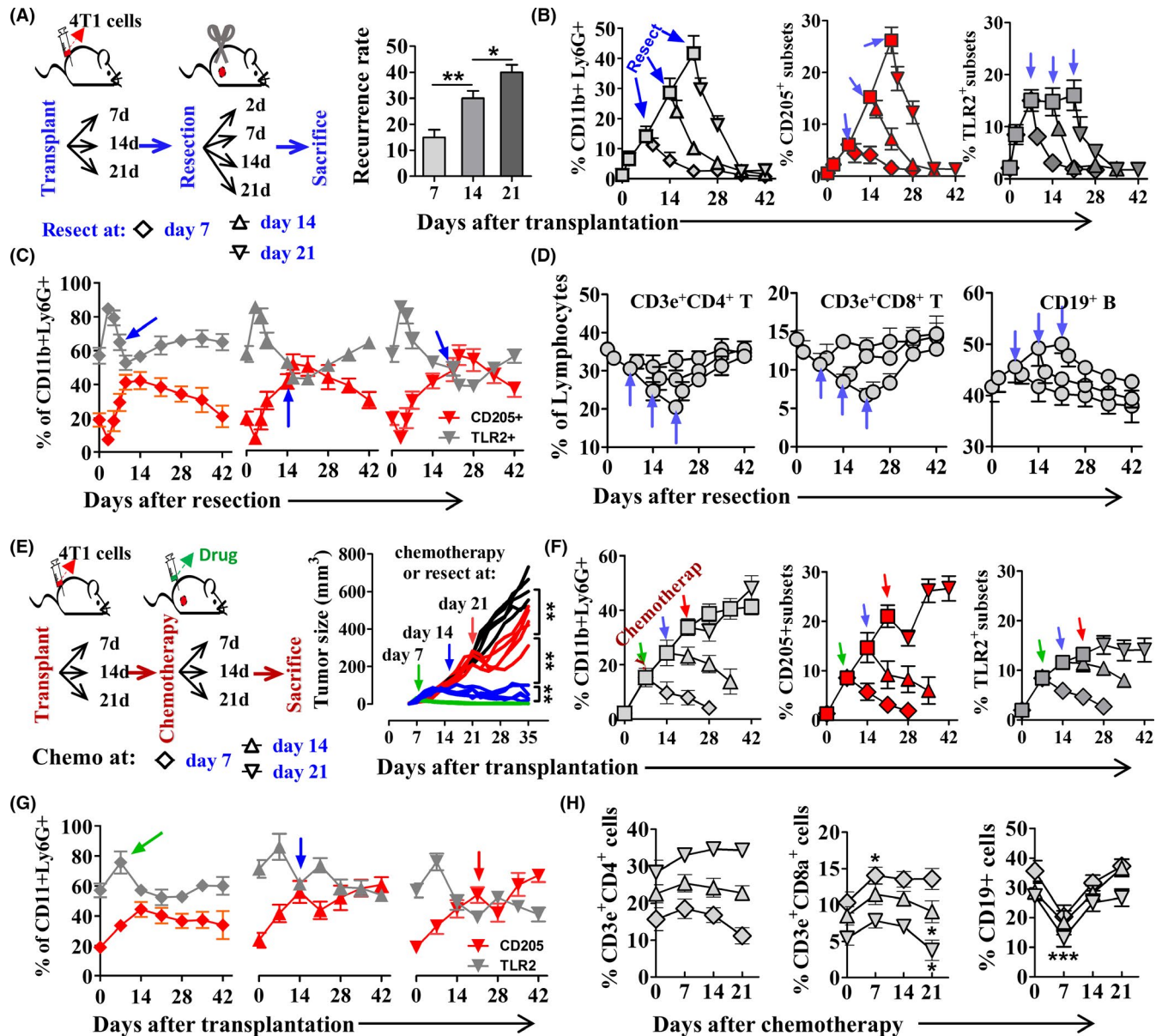


FIGURE 5 Dynamic characteristics of CD11b⁺Ly6G^{low}CD205⁺ in surgically resected and chemotherapeutically treated tumor-bearing mice. A–D, Mice were subcutaneously inoculated with or without 2×10^5 4T1 cells, and surgical resection was performed at the indicated time points. Splenic cells from tumor-bearing mice were collected for flow cytometry (FCM) analysis. A, Schematic diagram of the surgical resection protocol and the recurrence of in situ resected tumor-bearing mice. B, Proportion of total CD11b⁺Ly6G⁺ cells, CD11b⁺Ly6G^{low}CD205⁺ cells (CD205⁺ subsets), and CD11b⁺Ly6G^{high}TLR2⁺ cells (TLR2⁺ subsets) after resection. C, Ratio of CD205⁺ or TLR2⁺ subsets within CD11b⁺Ly6G⁺ cells. D, Percentage of CD3e⁺CD8⁺ T cells, CD3e⁺CD4⁺ T cells, and CD19⁺ B cells in the spleen of tumor-bearing mice. E–H, Mice were subcutaneously inoculated with or without 2×10^5 4T1 cells and underwent chemotherapy at the indicated time points. E, Schematic diagram of the chemotherapy protocol and the in situ tumor weight. F, Proportion of total CD11b⁺Ly6G⁺ cells, CD205⁺ subsets, and TLR2⁺ subsets after chemotherapy. G, Ratio of CD205⁺ or TLR2⁺ subsets within CD11b⁺Ly6G⁺ cells. H, Percentage of CD3e⁺CD8⁺ T cells, CD3e⁺CD4⁺ T cells, and CD19⁺ B cells in the spleen of tumor-bearing mice. Data represent ≥ 3 independent experiments and are shown as means \pm standard deviation. * $P < .05$, ** $P < .01$, *** $P < .001$, ns = significant, as determined by one-way ANOVA or Student *t* test

(Figure 7B). Intermittent fasting cycles effectively retard tumor growth²⁷ and keep blood glucose at a low level in 4T1 tumor-bearing mice.²⁸ Furthermore, in the same tumor model, we observed that intermittent fasting reduced the rate and number of CD205⁺ PM in the spleen (Figure 7C). Hence, GLUT3 can mediate apoptosis induced by glucose deficiency. To test this hypothesis, we applied siRNA technology to

block GLUT3 expression. The siRNA effectively blocked GLUT3 expression, reduced 2NBDG uptake and increased CD11b⁺Ly6G^{low}CD205⁺ cell apoptosis (Figure 7D,E). Furthermore, the CD11b⁺Ly6G⁺ cells (especially the CD205⁺ subsets) presented with downregulated GLUT3 and an upregulated caspase3/PARP apoptosis axis after GLUT3-siRNA treatment in vitro (Figure 7F).

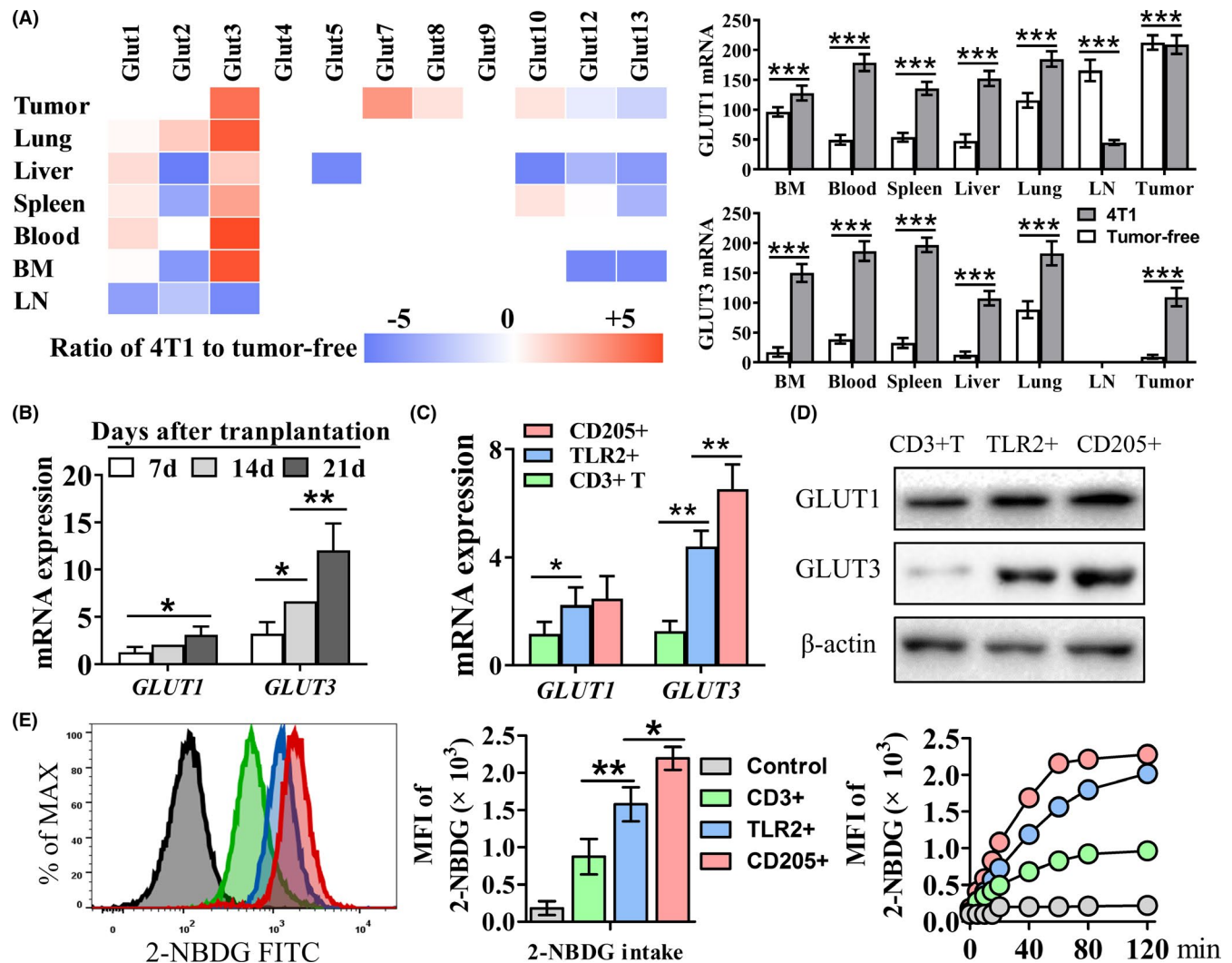


FIGURE 6 GLUT3 expression is directly correlated with increased glucose uptake in $\text{CD11b}^+\text{Ly6G}^{\text{low}}\text{CD205}^+$ cells. Mice were subcutaneously inoculated with or without 2×10^5 4T1 cells and euthanized after 3 wk. A, Various organs of tumor-bearing and tumor-free mice were collected to determine GLUT expression levels. Relative GLUT expression profiles (tumor-bearing/tumor-free) are shown in the heatmap. GLUT1 and GLUT3 expression detected with RT-PCR are shown in the bar diagram. B, Splenic leukocytes were collected from tumor-bearing mice at days 7, 14, and 21 post-transplantation and analyzed for GLUT1 and GLUT3 expression. Relative mRNA expression ($\text{GLUT1}/\beta\text{-actin}$) is shown in the bar diagram. C, D, Tumor-bearing mice were euthanized 3 wk post-transplantation, and splenic CD3^+ T cells (CD3^+ T), $\text{CD11b}^+\text{Ly6G}^{\text{high}}\text{TLR2}^+$ cells (TLR2^+), or $\text{CD11b}^+\text{Ly6G}^{\text{low}}\text{CD205}^+$ cells (CD205^+) were sorted through flow cytometry (FCM). C, Relative mRNA expression profiles ($\text{GLUT1}/\beta\text{-actin}$) are shown in the bar diagram. D, Western blots show GLUT1, GLUT3, and β -actin expression profiles in indicated cells. E, Tumor-bearing mice were euthanized 3 wk post-transplantation, and splenic leukocytes were collected to perform 2NBDG uptake assays. FCM histogram and bar diagram show the 2NBDG uptake profiles of the indicated cells. Line chart displays the 2NBDG uptake rates. Data represent ≥ 3 independent experiments and are shown as means \pm standard deviation. * $P < .05$, ** $P < .01$, *** $P < .001$, ns = significant, as determined by one-way ANOVA or Student t test

Overall, the foregoing results suggested that GLUT3 mediated $\text{CD11b}^+\text{Ly6G}^{\text{low}}\text{CD205}^+$ cell apoptosis induced by glucose deficiency and partially alleviated the MDSC-mediated antitumor immunosuppression.

4 | DISCUSSION

PMN-MDSCs are one of the vital factors that block antitumor immunity.¹ However, due to a lack of available biomarkers to distinguish

PMN-MDSC from neutrophils, both protumor and antitumor effects are observed in myeloid cells with $\text{CD11b}^+\text{Ly6G}^+$ phenotypes.^{4,7} In this paper, multiple criteria were used to characterize tumor-induced $\text{CD11b}^+\text{Ly6G}^+$ cell subpopulations (eg, cell surface markers, buoyancy, maturity, functions, and localization; please refer to Figure 8). Further observations showed that only CD205^+ PMN-MDSC supported tumor growth. We proved that the supportive function of CD205^+ PMN-MDSC relied on its suppression effects on T-cell proliferation. To deepen our understanding, we further metabolically characterized CD205^+ PMN-MDSCs and found that, under

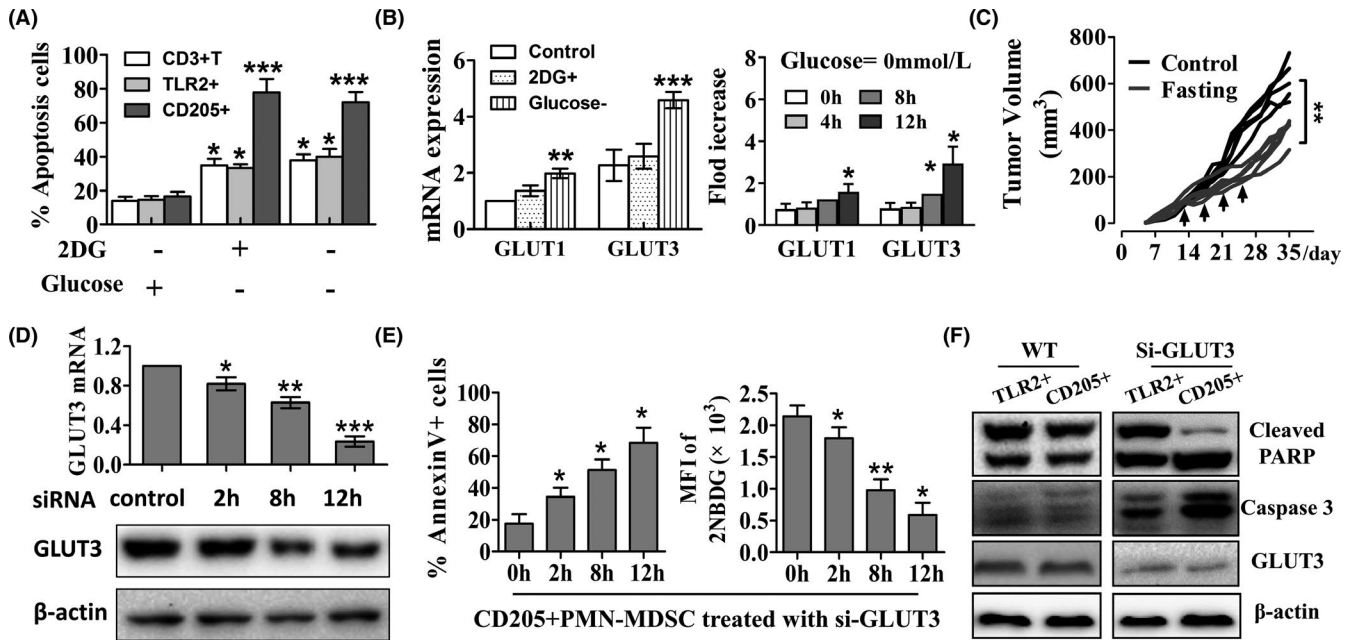


FIGURE 7 Blocking glucose metabolism induces CD11b⁺Ly6G^{low}CD205⁺ cell apoptosis in vitro. Tumor-bearing mice were euthanized 3 wk post-transplantation, and splenic CD3⁺ T cells (CD3⁺ T), CD11b⁺Ly6G^{high}TLR2⁺ cells (TLR2⁺), or CD11b⁺Ly6G^{low}CD205⁺ cells (CD205⁺) were sorted by flow cytometry (FCM). A, Glucose-free medium was used to culture sorted cells, and 10 mmol/L glucose or 2DG were added (or not added) to the medium of the in vitro cultured cells. The apoptosis rate of the cells was evaluated by annexin V/ 7-AAD staining. B, Sorted CD11b⁺Ly6G^{low}CD205⁺ cells were cultured in glucose-free medium (Glucose⁻) or in medium containing both 2DG and glucose (2DG⁺). Relative mRNA expression profiles (*GLUT1*/*β-actin*) are shown in the bar diagram. C, Tumor-bearing mice suffered 2 cycles of intermittent fasting treatment. The first cycle started on day 14 post-transplantation, the second cycle started on day 21, and each cycle lasted for 48–60 h. At the end of the second cycle, mice were euthanized for analysis. D, E, Sorted CD11b⁺Ly6G^{low}CD205⁺ cells were treated with GLUT3-siRNA in vitro. Both GLUT3 mRNA and protein expression profiles are shown in (D). Apoptosis rate and 2NBDG uptake rate are shown in (E). F, Sorted CD205⁺ and TLR2⁺ cells were treated with GLUT3-siRNA in vitro. Western blots show the expression profiles of cleaved-PARP, cleaved-caspase 3, and GLUT3. Data represent ≥ 3 independent experiments and are shown as means \pm standard deviation. * $P < .05$, ** $P < .01$, *** $P < .001$, ns = not significant, as determined by one-way ANOVA or Student *t* test

low glucose stress, the CD205⁺ PMN-MDSCs rapidly adapted by increasing GLUT3 expression (Figure 8). As GLUT3 has been recognized as a potential target for the rescue of host antitumor immunity, our results further highlighted the PMN-MDSC subsets within the CD205⁺GLUT3⁺ subpopulation as candidates for future targeting therapy.

Anti-Ly6C and anti-Ly6G antibodies are widely used biomarkers in tumor immunology to recognize MDSC subpopulations.²⁹ Furthermore, the correlation between Ly6G expression and granulocyte development has been described in numerous reports.¹ For instance, Evrard and colleagues identified a group of neutrophil precursors that shared the phenotype CD11b⁺Ly6G^{low}CXCR4⁻CXCR2⁺.³⁰ Kim and coworkers also defined a population of neutrophil precursor cells in the bone marrow, characterized by CD11b⁺Ly6G^{low}Ly6B^{int}CD115⁻.³¹ In the 2 reports above, neutrophil precursor cells showed ring-shaped nuclear morphology, proliferation potential, and the ability to develop into mature neutrophils. In addition, these neutrophil precursor cells expanded drastically in the bone marrow (BM) and spleen during inflammation and tumorigenesis. Similarly, in this study, we revealed that CD11b⁺Ly6G^{low}CD205⁺ was the minimum characteristic required to recognize the tumor-induced immunosuppressive, low-density,

and pre-mature PMN-MDSC subpopulations in murine breast tumor models (Figure 8). Furthermore, CD205⁺ PMN-MDSC had a similar CD marker expression profile with the above-mentioned neutrophil precursor cells, including CXCR4, CXCR2, CD16/32, CD43, and Gr-1 (Figures 1E and 4E). The dichotomy of PMN-MDSCs based on CD205 and TLR2 will help to better characterize tumor-induced granulocytes.

In this study, we observed that TLR2⁺ PMN-MDSCs maintained a weaker suppressive activity on T-cell proliferation (Figure 3B). As previously reported, TLR2 functions in myeloid cells involved both pro- and antitumor effects. In the B16 mouse melanoma tumor model, TLR2 acts as an essential receptor of diprovocim (an adjuvant reagent) for improving PD-1 antitumor effects.³² Meanwhile in the EG7 lymphoma tumor model, TLR2 signaling enhanced Mo-MDSC-mediated immunosuppression, which may downregulate an antitumor cytotoxic T-lymphocyte (CTL) response.³³ We observed that TLR2⁺ PMN-MDSC expressed a high level of B7-H1 (Figure 4E), a molecule that contributes to the immunosuppressive activity of PMN-MDSCs. These results suggested that the immunosuppression mechanism of PMN-MDSC depends on multiple negative regulatory factors. Consistently, in our 4T1 breast tumor model, TLR2 was also strongly expressed by M-MDSCs (Figure 4E), which have a

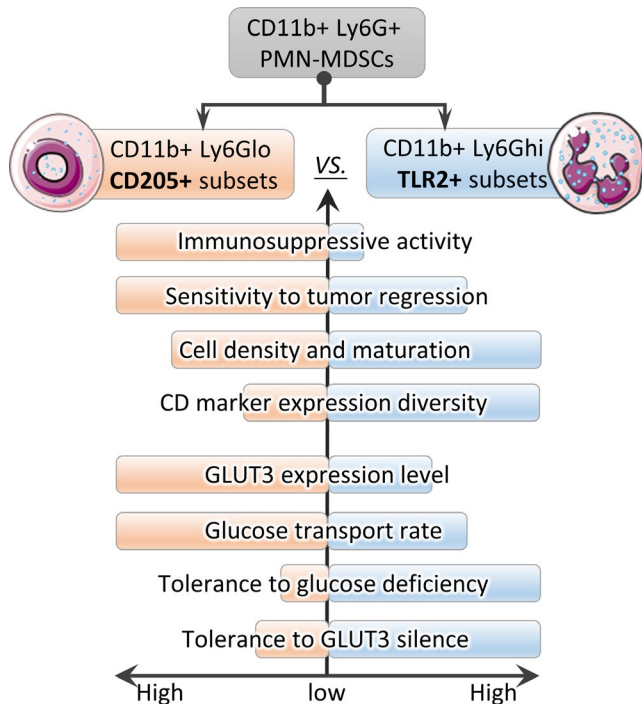


FIGURE 8 GLUT3 helps tumor-elicited suppressive CD205⁺ polymorphonuclear myeloid-derived suppressor cells (PMN-MDSCs) survive in a glucose-deficient environment. Cancer-induced PMN-MDSC comprise a group of heterogeneous cells. In this study, we propose a dichotomy of PMN-MDSCs based on CD205 and TLR2 expression. Furthermore, we observed that CD205⁺ PMN-MDSCs are sensitive to tumor regression induced by chemotherapy or tumor resection. We also showed that CD205⁺ PMN-MDSCs have potent immune-suppressive activity on T-cell proliferation. Moreover, CD205⁺ PMN-MDSCs have a lower cell density and reduced CD marker expression diversity. GLUT3 is selectively expressed by PMN-MDSC, especially CD205⁺ PMN-MDSC, and the survival of CD205⁺ PMN-MDSC is highly dependent on glucose metabolism and GLUT3 overexpression. The glucose-deficient environment challenge induced anergy of T cells in the spleen due to lack of efficient glucose transporters. In contrast, GLUT3 upregulation could help CD205⁺ PMN-MDSC cells uptake more glucose and reduce their apoptosis rate

potent immunosuppressive function on antitumor immunity. These observations suggested that TLR2 is involved in multiple immune responses, and the TLR2 function depends on specific pathological conditions and immune cell types.

CD205 (DEC205) is a type I transmembrane glycoprotein of the C-type lectin receptor family.³⁴ It is expressed at different levels in DC, B cells, T cells, and thymic epithelial cells.³⁵ CD205 is an endocytic receptor that can deliver antigen in DCs³⁵ or cancer cells³⁴ for presentation on MHC class I. Therefore, many researchers have generated much interest in the use of anti-CD205-antigen conjugates as therapeutic reagents. In addition, CD205 can mediate antigen tolerance in DCs by inducing deletion and unresponsiveness (anergy) in antigen-specific CD4⁺ and CD8⁺ T-cell populations,³⁶ and activating regulatory T-cell subsets.³⁷ Moreover, CD205 can also act as a recognition receptor for apoptotic and necrotic cells, potentially

providing an important pathway for self-antigen uptake in intra-thymic and peripheral tolerance.³⁵ RB6-8C5, an anti-Gr-1 mAb, has been widely used and considered effective in eliminating MDSC. A recent study reported that RB6-8C5-mediated anti-Gr-1 depletion failed to effectively remove hepatic MDSC, whereas it eliminated CD11b⁺Gr-1⁺ cells from the spleen and peripheral blood. RB6-8C5-bound MDSC retained immunosuppressive function and proliferation potential.³⁸ Regarding CD11b⁺Ly6G^{low}Gr-1^{low}CD205⁺ cells massively accumulated in the liver of tumor-bearing mice (Figure 4). CD205 molecules may prevent RB6-8C5-mediated CD11b⁺Gr-1⁺ cell depletion in the liver through antigen endocytosis. To the best of our knowledge, no previous report has described the function of CD205 molecules in granulocytes, therefore the function of DEC-205 remains poorly elucidated.

Previous reports have shown that infiltrating T cells compete with the tumor for nutrients, and highly glycolytic cancers can “starve” T cells of glucose.^{39,40} Incidentally, glucose depletion or competition by MDSCs may also account for the observed increases in T-cell anergy in tumor-bearing mice. Recently, Hsu et al⁴¹ and Rice et al⁴² reported that immature CD11b⁺Ly6G⁺ cells showed a high demand for glucose, indicating metabolic flexibility. Consequently, these cells have been reportedly involved in many different steps in the metastatic cascade of breast cancer via NETosis or reactive oxygen species (ROS) production. In such an environment (glucose deprivation), we showed that CD11b⁺Ly6G^{low}CD205⁺ cell survival depended on glucose uptake and GLUT3 overexpression (Figure 6). Moreover, massive apoptosis of CD11b⁺Ly6G^{low}CD205⁺ cells induced by 2DG treatment or GLUT3 knockdown revealed a fragility in these cells (Figure 7). The above-mentioned observations might explain why CD11b⁺Ly6G^{low}CD205⁺ cells did not accumulate massively in the tumor microenvironment (Figure 4A), where glucose depletion was extreme. Thus, we postulated that GLUT3 enhanced MDSC resistance to low glucose stress by competing for glucose and possibly preventing ROS-mediated MDSC apoptosis¹³ by glycolysis. Our results also demonstrated that GLUT1 and GLUT3 are strongly expressed, especially in the CD205⁺ PMN-MDSCs (Figure 6). Lymphocytes and 4T1 tumor cells expressed high GLUT1 and low GLUT3 levels, indicating that GLUT3 is specific to PMN-MDSC. GLUT3 may have a higher maximum glucose turnover rate than other Class 1 GLUT proteins.¹⁵ These findings and our observations suggested that GLUT3 is a putative target for the elimination of PMN-MDSCs. In practice, it is difficult to use gene-editing methods to explore the functions of PMN-MDSCs, as these cells have short lifespans.⁴³ Nevertheless, a GSK3 β inhibitor might selectively kill cancer cells overexpressing GLUT3, while scarcely affecting cells expressing only GLUT1.⁴⁴ Thus, we propose that GLUT3 inhibitors exhibit selective elimination of PMN-MDSCs. Identification of the GLUT3 regulators in PMN-MDSCs could help to elucidate the mechanisms by which PMN-MDSCs tolerate low glucose environments.

ACKNOWLEDGMENTS

This work was supported by the “Financial Support for Selected Researchers Back from Abroad (2012)” from Liaoning Province

(<http://www.ininfo.gov.cn/>) (Grant No. 88030312004). Flow cytometry and cell sorting were performed at the Cytometry and Cell Sorting Core at Shenyang Agriculture University, College of Animal Science and Veterinary Medicine with the expert assistance of Ran Chen.

CONFLICT OF INTEREST

The authors have no conflict of interest to declare.

ORCID

Shiliang Ma  <https://orcid.org/0000-0001-7143-0903>

REFERENCES

- Bronte V, Brandau S, Chen S-H, et al. Recommendations for myeloid-derived suppressor cell nomenclature and characterization standards. *Nat Commun*. 2016;7:12150.
- Oseroff A, Okada S, Strober S. Natural suppressor (NS) cells found in the spleen of neonatal mice and adult mice given total lymphoid irradiation (TLI) express the null surface phenotype. *J Immunol*. 1984;132(1):101-110.
- Movahedi K, Guillemins M, Van den Bossche J, et al. Identification of discrete tumor-induced myeloid-derived suppressor cell subpopulations with distinct T cell-suppressive activity. *Blood*. 2008;111(8):4233-4244.
- Youn JI, Collazo M, Shalova IN, Biswas SK, Gabrilovich DI. Characterization of the nature of granulocytic myeloid-derived suppressor cells in tumor-bearing mice. *J Leukoc Biol*. 2012;91(1):167-181.
- Porter CC, Druley TE, Erez A, et al. Recommendations for Surveillance for Children with Leukemia-Predisposing Conditions. *Clin Cancer Res*. 2017;23(11):E14-E22.
- Zhou J, et al. Neutrophils and PMN-MDSC: Their biological role and interaction with stromal cells. *Semin Immunol*. 2018;35:19-28.
- Herteman N, Vargas A, Lavoie J-P. Characterization of Circulating Low-Density Neutrophils Intrinsic Properties in Healthy and Asthmatic Horses. *Sci Rep*. 2017;7(1):1-10.
- Sagiv JY, Michaeli J, Assi S, et al. Phenotypic diversity and plasticity in circulating neutrophil subpopulations in cancer. *Cell Rep*. 2015;10(4):562-573.
- Condamine T, Dominguez GA, Youn J-I, et al. Lectin-type oxidized LDL receptor-1 distinguishes population of human polymorphonuclear myeloid-derived suppressor cells in cancer patients. *Sci Immunol*. 2016;1(2):aaf8943.
- Hanahan D, Weinberg RA. Hallmarks of cancer: the next generation. *Cell*. 2011;144(5):646-674.
- Vander Heiden MG, Locasale JW, Swanson KD, et al. Evidence for an alternative glycolytic pathway in rapidly proliferating cells. *Science*. 2010;329(5998):1492-1499.
- Li W, Tanikawa T, Kryczek I, et al. Aerobic glycolysis controls myeloid-derived suppressor cells and tumor immunity via a specific CEBPB isoform in triple-negative breast cancer. *Cell Metab*. 2018;28(1):87-103.e6.
- Jian SL, Chen W-W, Su Y-C, et al. Glycolysis regulates the expansion of myeloid-derived suppressor cells in tumor-bearing hosts through prevention of ROS-mediated apoptosis. *Cell Death Dis*. 2017;8(5):e2779.
- Veglia F, Tyurin VA, Blasi M, et al. Fatty acid transport protein 2 reprograms neutrophils in cancer. *Nature*. 2019;569(7754):73-78.
- Mueckler M, Thorens B. The SLC2 (GLUT) family of membrane transporters. *Mol Aspects Med*. 2013;34(2-3):121-138.
- Euhus DM, Hudd C, Laregina MC, Johnson FE. Tumor measurement in the nude mouse. *J Surg Oncol*. 1986;31(4):229-234.
- Bossuyt X, Marti GE, Fleisher TA. Comparative analysis of whole blood lysis methods for flow cytometry. *Cytometry*. 1997;30(3):124-133.
- Brandau S, Dumitru CA, Lang S. Protumor and antitumor functions of neutrophil granulocytes. *Semin Immunopathol*. 2013;35(2):163-176.
- Mantovani A, Cassatella MA, Costantini C, Jaillon S, et al. Neutrophils in the activation and regulation of innate and adaptive immunity. *Nat Rev Immunol*. 2011;11(8):519-531.
- Peranzoni E, Zilio S, Marigo I, et al. Myeloid-derived suppressor cell heterogeneity and subset definition. *Curr Opin Immunol*. 2010;22(2):238-244.
- Salvadori S, Martinelli G, Zier K. Resection of solid tumors reverses T cell defects and restores protective immunity. *J Immunol*. 2000;164(4):2214-2220.
- Piranlioglu R, Lee E, Ouzounova M, et al. Primary tumor-induced immunity eradicates disseminated tumor cells in syngeneic mouse model. *Nat Commun*. 2019;10(1):1430.
- Predina JD, Kapoor V, Judy BF, et al. Cytoablation surgery reduces systemic myeloid suppressor cell populations and restores intratumoral immunotherapy effectiveness. *J Hematol Oncol*. 2012;5:34.
- Alizadeh D, Trad M, Hanke NT, et al. Doxorubicin eliminates myeloid-derived suppressor cells and enhances the efficacy of adoptive T-cell transfer in breast cancer. *Cancer Res*. 2014;74(1):104-118.
- DuPre SA, Hunter KW Jr. Murine mammary carcinoma 4T1 induces a leukemoid reaction with splenomegaly: association with tumor-derived growth factors. *Exp Mol Pathol*. 2007;82(1):12-24.
- Youn JI, Gabrilovich DI. The biology of myeloid-derived suppressor cells: the blessing and the curse of morphological and functional heterogeneity. *Eur J Immunol*. 2010;40(11):2969-2975.
- Lee C, Raffaghello L, Brandhorst S, et al. Fasting cycles retard growth of tumors and sensitize a range of cancer cell types to chemotherapy. *Sci Transl Med*. 2012;4(124):124ra27.
- Nencioni A, Caffa I, Cortellino S, Longo VD. Fasting and cancer: molecular mechanisms and clinical application. *Nat Rev Cancer*. 2018;18(11):707-719.
- Youn JI, Nagaraj S, Collazo M, Gabrilovich DI. Subsets of myeloid-derived suppressor cells in tumor-bearing mice. *J Immunol*. 2008;181(8):5791-5802.
- Evrard M, Kwok IWH, Chong SZ, et al. Developmental Analysis of Bone Marrow Neutrophils Reveals Populations Specialized in Expansion, Trafficking, and Effector Functions. *Immunity*. 2018;48(2):364-379.e8.
- Kim M-H, Yang D, Kim M, Kim S-Y, Kim D, Kang S-J. A late-lineage murine neutrophil precursor population exhibits dynamic changes during demand-adapted granulopoiesis. *Sci Rep*. 2017;7(1):39804.
- Wang Y, Su L, Morin MD, et al. Adjuvant effect of the novel TLR1/TLR2 agonist Diprovocim synergizes with anti-PD-L1 to eliminate melanoma in mice. *Proc Natl Acad Sci USA*. 2018;115(37):E8698-E8706.
- Shime H, Maruyama A, Yoshida S, Takeda Y, Matsumoto M, Seya T. Toll-like receptor 2 ligand and interferon-gamma suppress anti-tumor T cell responses by enhancing the immunosuppressive activity of monocytic myeloid-derived suppressor cells. *Oncoimmunology*. 2018;7(1):e1373231.
- Merlino G, Fiascarelli A, Bigioni M, et al. MEN1309/OBT076, a First-In-Class Antibody-Drug Conjugate Targeting CD205 in Solid Tumors. *Mol Cancer Ther*. 2019;18(9):1533-1543.
- Caminschi I, Meuter S, Heath WR. DEC-205 is a cell surface receptor for CpG oligonucleotides. *Oncoimmunology*. 2013;2(3):e23128.
- Bonifaz L, Bonnyay D, Mahnke K, et al. Efficient targeting of protein antigen to the dendritic cell receptor DEC-205 in the steady state leads to antigen presentation on major histocompatibility complex class I products and peripheral CD8+ T cell tolerance. *J Exp Med*. 2002;196(12):1627-1638.

37. Mahnke K, Qian Y, Knop J, Enk AH. Induction of CD4⁺/CD25⁺ regulatory T cells by targeting of antigens to immature dendritic cells. *Blood*. 2003;101(12):4862-4869.
38. Ma C, Kapanadze T, Gamrekelashvili J, Manns MP, Korangy F, Greten TF. Anti-Gr-1 antibody depletion fails to eliminate hepatic myeloid-derived suppressor cells in tumor-bearing mice. *J Leukoc Biol*. 2012;92(6):1199-1206.
39. Ibanez-Vea M, Ghorghanlu S, Ahmadi-Khiavi H, et al. Myeloid-Derived Suppressor Cells in the Tumor Microenvironment: Current Knowledge and Future Perspectives. *Arch Immunol Ther Exp (Warsz)*. 2018;66(2):113-123.
40. Chang CH, Qiu J, O'Sullivan D, et al. Metabolic Competition in the Tumor Microenvironment Is a Driver of Cancer Progression. *Cell*. 2015;162(6):1229-1241.
41. Hsu BE, Tabariès S, Johnson RM, et al. Immature low-density neutrophils exhibit metabolic flexibility that facilitates breast cancer liver metastasis. *Cell Rep*. 2019;27(13):3902-3915.e6.
42. Rice CM, Davies LC, Subleski JJ, et al. Tumour-elicited neutrophils engage mitochondrial metabolism to circumvent nutrient limitations and maintain immune suppression. *Nat Commun*. 2018;9(1):5099.
43. McCracken JM, Allen LA. Regulation of human neutrophil apoptosis and lifespan in health and disease. *J Cell Death*. 2014;7:15-23.
44. Watanabe M, Abe N, Oshikiri Y, Stanbridge EJ, Kitagawa T. Selective growth inhibition by glycogen synthase kinase-3 inhibitors in tumorigenic HeLa hybrid cells is mediated through NF-kappaB-dependent GLUT3 expression. *Oncogenesis*. 2012;1:e21.

SUPPORTING INFORMATION

Additional supporting information may be found online in the Supporting Information section.

How to cite this article: Fu C, Fu Z, Jiang C, et al. CD205⁺ polymorphonuclear myeloid-derived suppressor cells suppress antitumor immunity by overexpressing GLUT3. *Cancer Sci*. 2021;112:1011-1025. <https://doi.org/10.1111/cas.14783>